PAPER

Atomic-scale changes of silica-supported catalysts with nanocrystalline or amorphous gallia phases: implications of hydrogen pretreatment on their selectivity for propane dehydrogenation†

Pedro Castro-Fernández, [iD] [a] Alexander I. Serykh,[b] Alexander V. Yakimov,[c] Igor P. Prosvirin,[d] Andrey V. Bukhtiyarov, [iD] [d] Paula M. Abdala, [iD] *[a] Christophe Copéret, [iD] [c] Alexey Fedorov [iD] *[a] and Christoph R. Müller [iD] *[a]

This work explores how H_2 pretreatment at 550 °C induces structural transformation of two gallia-based propane dehydrogenation (PDH) catalysts, *viz.* nanocrystalline γ/β-Ga_2O_3 and amorphous Ga_2O_3 (GaO_x) supported on silica (γ-Ga_2O_3/SiO_2 and Ga/SiO_2, respectively) and how it affects their activity, propene selectivity and stability with time on stream (TOS). Ga/SiO_2–H_2 shows poor activity and propene selectivity, no coking and no deactivation with TOS, similar to Ga/SiO_2. In contrast, the high initial activity and propene selectivity of γ-Ga_2O_3/SiO_2–H_2 decline with TOS but to a lesser extent than in calcined γ-Ga_2O_3/SiO_2. In addition, γ-Ga_2O_3/SiO_2–H_2 cokes less than γ-Ga_2O_3/SiO_2. Ga K-edge X-ray absorption spectroscopy suggests an increased disorder of the nanocrystalline γ/β-Ga_2O_3 phases in γ-Ga_2O_3/SiO_2–H_2 and the emergence of additional tetrahedral Ga sites (Ga_{IV}). Such Ga_{IV} sites are strong Lewis acid sites (LAS) according to studies using adsorbed pyridine and CO probe molecules, *i.e.*, the abundance of strong LAS is higher in γ-Ga_2O_3/SiO_2–H_2 compared to γ-Ga_2O_3/SiO_2 but lower than in Ga/SiO_2 and Ga/SiO_2–H_2. Dissociation of H_2 on the Ga–O linkages in γ-Ga_2O_3/SiO_2–H_2 yields high-frequency Ga–H bands that are observed in Ga/SiO_2 and Ga/SiO_2–H_2 but not detected in γ-Ga_2O_3/SiO_2. We attribute the increased amount of Ga_{IV} sites in γ-Ga_2O_3/SiO_2–H_2 mostly to an increased disorder in γ/β-Ga_2O_3. X-ray photoelectron spectroscopy detects the formation of Ga^+ and Ga^0 species in both Ga/SiO_2–H_2 and γ-Ga_2O_3/SiO_2–H_2. Therefore, it is likely that a minor amount of Ga_{IV} sites also forms through the interaction of Ga^+ (such as Ga_2O) and/or Ga^0 with silanol groups of SiO_2.

Introduction

The industrial production of propene through propane dehydrogenation (PDH) relies mainly on $PtSn$/Al_2O_3 or CrO_x/Al_2O_3 catalysts, yet the high cost of Pt and the environmental toxicity of Cr^{6+} has motivated the search for alternative catalyst formulations.[1–5] Among the alternatives explored, Ga-based catalysts are considered promising. For instance, a Ga/H-ZSM-5 zeolite catalyst has been used for the Cyclar propane aromatization process, in which the dehydrogenation of propane to propene proceeds on Ga-based active sites, followed by dehydrogenative aromatization of propene on the strong Brønsted acid sites of the zeolite.[6,7] Furthermore, the FCDh (fluidized catalytic dehydrogenation of propane) process, which uses a $PtGa$/Al_2O_3 catalyst is currently at the initial phase of its industrial deployment.[8]

A reductive pretreatment of zeolitic Ga-based catalysts under H_2 at 450–650 °C is often used to increase the activity and selectivity of the Ga-based active sites for propane dehydrogenation.[9] It has been demonstrated that the dispersion of Ga in mechanically mixed Ga_2O_3/H-ZSM-5 catalysts increases under H_2 pretreatment conditions, explained by the formation of reduced Ga species that diffuse within the zeolitic channels and anchor onto acidic hydroxyl groups.[10] Various reduced zeolitic Ga species have been proposed to form after reductive pretreatment or under reaction conditions, and, presumably, also the reduced species are active in PDH.[11–13] H_2 pretreatment of Ga/H-ZSM-

[a] Department of Mechanical and Process Engineering, ETH Zürich, CH-8092, Zürich, Switzerland. E-mail: abdalap@ethz.ch, fedoroal@ethz.ch, muelchri@ethz.ch
[b] Zelinsky Institute of Organic Chemistry, RAS, Moscow, 119991, Russia
[c] Department of Chemistry and Applied Biosciences, ETH Zürich, CH-8093, Zürich, Switzerland
[d] Boreskov Institute of Catalysis, SB RAS, 630090 Novosibirsk, Russia

† Electronic supplementary information (ESI) available: Experimental procedures, XAS, FTIR, STEM-EDX, XPS, dPDF and ^{15}N DNP SENS experimental parameters. See DOI: https://doi.org/10.1039/d2cy00074a

This journal is © The Royal Society of Chemistry 2022

Catal. Sci. Technol., 2022, **12**, 3957–3968 | **3957**

5 and Ga/H-MFI zeolites, followed by *in situ* X-ray absorption near edge structure spectroscopy (XANES) experiments at the Ga K-edge showed a shift in the absorption edge to lower energies (~4.6 eV (ref. 14)) that has been related to the reduction of Ga^{3+} to Ga^+, which then may quickly reoxidize to form GaO^+ or $[GaH_2]^+$ species.[11,14–16] The conclusions from XANES experiments have been supported by X-ray photoelectron spectroscopy (XPS) studies of Ga zeolites that revealed Ga 3d features at lower binding energies relative to the Ga^{3+} peaks; such features have been ascribed to Ga^+, $Ga^{\delta+}$ and metallic Ga.[17]

That being said, the interaction of the gallia phase with silica, a typical non-microporous support, and the nature of the Ga sites formed in such supported materials under H_2 treatment remains less explored. Treatment of a Ga_2O_3/SiO_2 catalyst with H_2 at 550 °C has been reported to lead to a partial reduction of Ga_2O_3, lower propene yields in PDH and higher yields to aromatics, the latter observation explained by an increase in the number of Brønsted acid sites.[18] Similar to the reduction of Ga^{3+} sites in zeolites, it has been shown that H_2 pretreatment at 550 °C of a Ga_2O_3/SiO_2 material gave XPS features consistent with Ga^+ species.[19] In another report, Ga K-edge XANES and XPS analysis of a Ga_2O_3/SiO_2 catalyst treated with H_2 at 650 °C also suggested the presence of reduced Ga sites.[20] However, after H_2 pretreatment, the latter catalyst showed a loss of PDH activity, suggested to be due to the formation of lower-coordinated $Ga^{\delta+}$ species.[20] Additionally, the emergence of a low-energy XANES edge feature has been observed when comparing fresh and used (after 20 hours of time on stream, TOS) single site $[(\equiv SiO)_3Ga(XOSi\equiv)]$ (where X is H or $\equiv Si$) PDH catalyst,[21] prepared by the surface organometallic chemistry approach.[22] The low energy edge feature in the XANES spectra may be associated with the reduction of Ga sites; however, recent evidence from reference molecular alkyl gallium compounds suggests that such feature may, at least in part, be associated with the formation of Ga alkyl surface species during the PDH reaction.[23] This evidence is in line with a further report that demonstrated that an edge feature at lower energies in the Ga K-edge XANES spectra could be due to changes in the coordination number and/or formation of gallium hydride and alkyl species.[24]

Studies of unsupported gallia catalysts have suggested that the high activity of β-Ga_2O_3 in PDH (as compared to other gallia polymorphs) is due to the high relative fraction of weak Lewis acid sites (LAS) on the surface of β-Ga_2O_3.[25] It has been shown that oxygen vacancy (V_o) surface sites in β-Ga_2O_3 can be generated by H_2 pretreatment.[26] Density functional theory studies on a dehydroxylated model surface of β-Ga_2O_3 have ascribed weak LAS to tricoordinated Ga^{3+} sites, that is, Ga sites in tetrahedral surface termination positions that neighbor V_o surface sites.[25] The relevance of weak Ga-based LAS in unsupported nanoparticle catalysts for a high activity in PDH has also been supported by structure–performance relationship studies of mixed oxide $(Ga,Al)_2O_3$ catalysts.[27,28]

In this work, we compare the structural changes of two gallia based, silica-supported catalysts upon H_2 pretreatment,

with one material containing a nanocrystalline, and another one an amorphous gallia phase, denoted γ-Ga_2O_3/SiO_2 and Ga/SiO_2, respectively (with similar Ga loadings of 2–3 wt%). The calcined materials have been characterized by us in detail previously.[25] Ga/SiO_2 and γ-Ga_2O_3/SiO_2 display different reducibility under H_2 treatment. More specifically, Ga/SiO_2, a PDH catalyst with a low activity and selectivity owing to the undesired cracking of propane on unselective Ga sites and, possibly, also on strong Brønsted acid sites (BAS, due to a small amount of gallosilicate sites in Ga/SiO_2), shows no notable changes in its PDH performance after H_2 treatment at 550 °C (2 h). In contrast, γ-Ga_2O_3/SiO_2 displays, after the same reductive pretreatment, a higher stability with TOS both with regards to its activity and even more notably in its propene selectivity. The *in situ* X-ray absorption spectroscopy (XAS) study of γ-Ga_2O_3/SiO_2 at the Ga K-edge complemented by quasi *in situ* XPS suggests a higher reducibility of the nanocrystalline gallia phase in γ-Ga_2O_3/SiO_2 relative to the amorphous gallia phase in Ga/SiO_2. Upon H_2 treatment we observe an increased disorder of the nanocrystalline gallia phase in γ-Ga_2O_3/SiO_2–H_2 that occurs in parallel with the reduction of Ga^{3+} sites to Ga^+ and Ga^0 species and the emergence of additional tetrahedral Ga sites (Ga_{IV}). According to surface acidity studies using pyridine and CO probe molecules, the newly formed Ga_{IV} sites feature strong Lewis acidity, similarly to the acidity of the LAS in the amorphous gallia catalysts Ga/SiO_2 and Ga/SiO_2–H_2, while avoiding the formation of strong BAS. In addition to the explanation given above, it is conceivable that Ga^+ and/or Ga^0 species interact with and anchor onto silanols groups of the silica support.

Materials and methods

Materials

The synthesis and structural characterization of the γ-Ga_2O_3/SiO_2 and Ga/SiO_2 catalysts have been described by us previously.[25] In brief, γ-Ga_2O_3/SiO_2 and Ga/SiO_2 were obtained by the incipient wetness impregnation of amorphous silica with a colloidal solution of γ-Ga_2O_3 nanoparticles in toluene (particle diameter 2.5 ± 0.6 nm) or an aqueous solution of $Ga(NO_3)_3$, respectively, followed by drying and calcination (600 °C, 2 h). γ-Ga_2O_3/SiO_2–H_2 and Ga/SiO_2–H_2 were obtained by pretreating γ-Ga_2O_3/SiO_2 and Ga/SiO_2 in undiluted H_2 at 550 °C for 2 h (10 °C min^{-1}).

Catalytic testing

Propane dehydrogenation tests were carried out in a benchtop Microactivity EFFI reactor (PID Eng&Tech). A mass of 50 mg of catalyst was mixed with 1.20 g of SiC (46 grit, Alfa-Aesar), and placed, between two plugs of quartz wool, onto a frit of a quartz fixed-bed reactor (diameter 13 mm). After reaching the reaction temperature (550 °C, 10 °C min^{-1}) under a flow of N_2, a mixture of 10% C_3H_8 diluted in N_2 was

3958 | *Catal. Sci. Technol.*, 2022, **12**, 3957–3968

This journal is © The Royal Society of Chemistry 2022

introduced into the reactor (weight hourly space velocity, WHSV = 7.2 h^{-1}). The composition of the outlet gasses was analyzed using a gas chromatograph (Clarus 480, PerkinElmer) with a flame ionization detector and a thermal conductivity detector. The first sampling of the gasses was made after 4 min of reaction, collecting data for every 20 minutes afterwards. For the H$_2$-treated catalysts, before PDH reaction, the catalysts were heated up under H$_2$ to 550 °C (50 mL min^{-1}), and held at this temperature for 2 hours. Subsequently, the catalyst bed was flushed with N$_2$ for 15 min before switching to a C$_3$H$_8$/N$_2$ mixture.

Thermogravimetric analyses

For thermogravimetric analyses (TGA), *ca.* 15 mg of the catalyst were placed in a 70 μL alumina crucible and introduced into the instrument (DSC 1, Mettler-Toledo). The material was heated to 550 °C (10 °C min^{-1}) under a N$_2$ flow of 75 mL min^{-1} (of which 25 mL min^{-1} correspond to the purge flow of the balance). After having reached the desired temperature and holding at this temperature for 10 min, 10% of propane (7.5 mL min^{-1}) was introduced to the N$_2$ flow. Changes in the catalyst weight were monitored for 160 min.

XAS and X-ray total scattering

X-ray absorption measurements were performed at the Swiss-Norwegian beamlines (SNBL, BM31) at the European Synchrotron Radiation Facility (ESRF).[29] Spectra were obtained at the Ga K-edge in transmission mode (continuous scanning), using a double-crystal Si(111) monochromator. For *ex situ* measurements, the materials were mixed with an optimal amount of cellulose and pressed into self-supporting pellets.[30] Pellets of H$_2$-treated materials were prepared inside of a glovebox and kept in air-tight sealed bags for measurements.

In situ XAS experiments were carried out in a quartz capillary reactor (diameter 1 mm; wall thickness = 0.1 mm) whereby the catalyst was placed between two quartz wool plugs. H$_2$ was flowed (10 mL min^{-1}) through the reactor while heating up from room temperature to 550 °C (10 °C min^{-1}) using an air blower. During cooling down the reactor was flushed with He. A schematics of the XAS setup has been described in a previous publication.[25] Data processing was carried out using the DEMETER software suite.[31] Energy calibration was performed using a Zn-foil. Data processing was done using the Athena software.[30] FEFF paths and the amplitude reduction factor (S_0^2) were generated by the Artemis software using a β-Ga$_2$O$_3$ structural model.[31,32]

X-ray total scattering data were collected at BM31 in a consecutive (combined) mode to the *in situ* XAS data. Data collection was performed before and after H$_2$ treatment at 50 °C, using a wavelength of λ = 0.25811 Å (set by a double-crystal Si(111) monochromator), and a two-dimensional MAR detector (MAR345 image plate). The data collection time was 20 min. To obtain pair distribution functions (PDF, G(r)) from

the supported gallia phase, the scattering signal was subtracted from the scattering signal of the pure SiO$_2$ support.[33] PDFs were obtained using the PDFgetX3 software,[34] setting a Q_{max} = 16 Å^{-1} and a R_{poly} = 1.6.

Dynamic nuclear polarization surface enhanced nuclear resonance spectroscopy (DNP SENS)

Prior to NMR measurements, γ-Ga$_2$O$_3$/SiO$_2$–H$_2$ and Ga/SiO$_2$–H$_2$ were dehydroxylated at 550 °C at *ca.* 10^{-5} mbar for 2 h (3 °C min^{-1}). Subsequently, the materials were exposed for 20 min at room temperature to the saturated vapor pressure of ^{15}N labelled pyridine (Py), followed by evacuation at 150 °C at *ca.* 10^{-5} mbar for 15 min. Before use, ^{15}N Py was dried by adding CaH$_2$ and stirring at 60 °C for 72 h. Afterwards, the solution was degassed by several freeze–pump–thaw cycles.[22] Materials with pre-adsorbed Py were impregnated in a glovebox (O$_2$ and H$_2$O < 1 ppm) with a 16 mM TEKPol in 1,1,2,2-tetrachloroethane (TCE) solution.[35,36] The impregnated materials were introduced into a sapphire rotor (outer diameter 3.2 mm), and closed with a zirconia cap. The rotor was placed quickly in a cold NMR probe (100 K). ^{15}N DNP SENS spectra were acquired on a Bruker 600 MHz (14.1 T) instrument equipped with a 3.2 mm Bruker low-temperature double-resonance probe coupled to a 395 GHz gyrotron microwave source (output power = 6–10 W) to drive the DNP cross-effect. In all experiments a MAS rate of 8 kHz was used. DNP-enhanced ^{15}N NMR spectra were measured using a {^{1}H}^{15}N CPMAS pulse sequence with the contact time of 2 ms. As a reference for the static magnetic field, the ^{13}C higher-frequency peak of adamantane at 38.4 ppm was used. The DNP buildup time (τ_{DNP}) was measured by a ^{1}H saturation-recovery experiment with the microwaves turned on. A summary of the experimental DNP SENS parameters are given in Table S1.†

XPS

X-ray photoelectron spectra were recorded on a SPECS photoelectron spectrometer using a hemispherical PHOIBOS 150 MCD 9 analyzer (AlK$_a$ radiation, hv = 1486.6 eV, 150 W). The binding energy (BE) scale was pre-calibrated using the positions of the peaks of the Au 4f$_{7/2}$ (BE = 84.0 eV) and Cu2p$_{3/2}$ (BE = 932.67 eV) core levels. The Si 2p peak at 103.5 eV of the SiO$_2$ support was used as an internal standard. The survey spectra were recorded at a pass energy of 50 eV, and for the narrow spectral regions at 20 eV. To determine the chemical (charge) state of elements on the surface of the materials, the regions of Ga 3d and O 2s, Si 2p, Si 2s, C 1s, O 1s, Ga 2p$_{3/2}$ were measured. The atomic ratios of the elements on the catalyst surface were calculated from the integral photoelectron peak intensities which were corrected by theoretical sensitivity factors based on Scofield's photoionization cross sections.[37] The residual gas pressure during the measurements did not exceed 8 × 10^{-9} mbar. To carry out experiments using the high pressure cell (HPC) of

This journal is © The Royal Society of Chemistry 2022

Catal. Sci. Technol., 2022, **12**, 3957–3968 | **3959**

the SPECS photoelectron spectrometer, all materials were rubbed into a stainless steel mesh that was spot welded onto a standard holder. HPC allows to pretreat the specimen under different gases at pressures up to 1 bar and in the temperature range from 50 to 450 °C. The pretreatment was performed for 1 h at a hydrogen pressure of *ca.* 300 mbar either at 300 °C or 450 °C, followed by an outgassing to UHV conditions at the respective pretreatment temperature. The pretreated materials were transferred to the analyzer chamber without any contact with air. Additional XPS data (survey scans, C 1s, Si 2p, Ga 3d, O 2s and Ga LMM lines) are presented in Fig. S4 and S5.†

Fourier-transform infrared spectroscopy (FTIR)

Infrared spectra were recorded on a Nicolet Protege 360 spectrophotometer in transmittance mode (spectral resolution 4 cm^{-1}). Powdered materials were pressed into self-supporting wafers (15–20 mg cm^{-2}) and placed into a vacuum infrared quartz cell equipped with CaF$_2$ windows. The dissociative adsorption of hydrogen (*ca.* 1–2 min hydrogen exposure time) was studied at different temperatures (300, 450 and 540 °C) at an equilibrium hydrogen pressure of *ca.* 70 mbar on both calcined materials and on the materials treated in hydrogen. Calcined and H$_2$-treated materials before hydrogen adsorption were outgassed at 813 K for 2 h in a medium vacuum of *ca.* 10^{-3} mbar. The hydrogen pretreatment of the self-supporting wafers was conducted in the IR cell under static conditions (three cycles of exposure of the specimen to *ca.* 130 mbar of H$_2$ for 0.5 h with evacuation to *ca.* 10^{-3} mbar in-between the H$_2$ exposures). The IR spectra were measured at room temperature. Both calcined and H$_2$-treated materials were also characterized by the adsorption of CO. The adsorption of CO was conducted at room temperature and an equilibrium pressure of *ca.* 27 mbar.

Scanning transmission electron microscopy – energy dispersive X-ray spectroscopy (STEM-EDX)

Materials were dispersed on a copper grid and analyzed using a FEI Talos F200X instrument. The operation voltage was set to 200 kV in scanning transmission electron microscopic (STEM) mode. EDX was performed using an accelerating voltage of 40 keV.

Fig. 1, 2, S2 and S7,† and Table 1 present results for calcined γ-Ga$_2$O$_3$/SiO$_2$ and Ga/SiO$_2$ catalysts. This data has been reported by us in ref. 25 and is reproduced here for comparison to γ-Ga$_2$O$_3$/SiO$_2$–H$_2$ and Ga/SiO$_2$–H$_2$, with permission from the American Chemical Society (Copyright 2021).

Results

Catalytic performance and coking

γ-Ga$_2$O$_3$/SiO$_2$ and Ga/SiO$_2$ are PDH catalysts that contain dispersed nanocrystalline gallia nanoparticles (NPs, γ/β-phase Ga$_2$O$_3$) and a mostly XRD-amorphous gallia phase with a
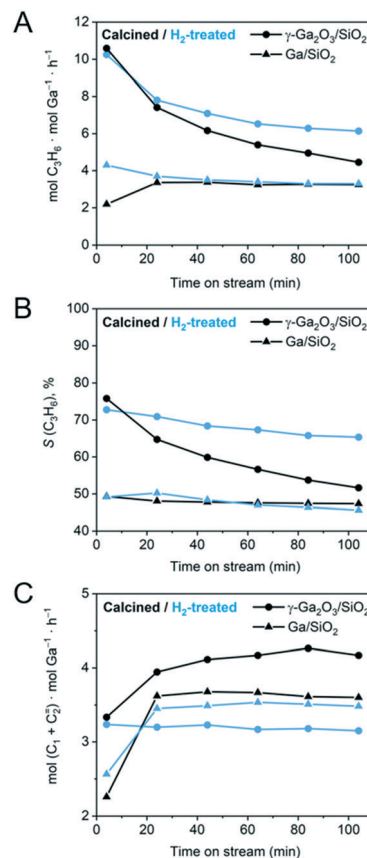

Fig. 1 Results of the PDH catalytic tests for calcined (black traces) and H$_2$-treated (blue traces) γ-Ga$_2$O$_3$/SiO$_2$ and Ga/SiO$_2$. (A) Ga-Normalized formation rate of propene, (B) selectivity to propene, and (C) Ga-normalized formation rates of cracking products (methane and ethene). Catalytic data for the calcined γ-Ga$_2$O$_3$/SiO$_2$ and Ga/SiO$_2$ has been reported by us previously and is reproduced here for comparison.[25]

short range order (*ca.* 5 Å), respectively.[25,38] These two catalysts were treated in undiluted H$_2$ at 550 °C for 2 h prior to their catalytic PDH tests at 550 °C for 104 min at a WHSV = 7.2 h^{-1}. Note that the catalytic results for γ-Ga$_2$O$_3$/SiO$_2$ and Ga/SiO$_2$ have been reported by us previously,[25] and are plotted in Fig. 1 to allow a comparison with the H$_2$-treated materials. Fig. 1A displays propene formation rates normalized per ICP-determined Ga loading. Fig. 1B and C present the selectivity to propene and Ga-normalized formation rates of the cracking products (methane and ethene), respectively.

The initial activity and selectivity to propene (after 4 min TOS) of γ-Ga$_2$O$_3$/SiO$_2$–H$_2$ are 10.3 mol C$_3$H$_6$ mol Ga^{-1} h^{-1} and 72%, respectively, which are similar to γ-Ga$_2$O$_3$/SiO$_2$. However, the decrease of the activity and selectivity of γ-Ga$_2$O$_3$/SiO$_2$–H$_2$ after 104 min TOS is lower than that in γ-Ga$_2$O$_3$/SiO$_2$ (Fig. 1A). The higher propene selectivity of γ-Ga$_2$O$_3$/SiO$_2$–H$_2$ relative to γ-Ga$_2$O$_3$/SiO$_2$ correlates with the decreased rate of cracking to methane and ethene, *i.e.* ca. 4.2 mol (CH$_4$ + C$_2$H$_4$) mol Ga^{-1} h^{-1} for γ-Ga$_2$O$_3$/SiO$_2$ and 3.2 mol (CH$_4$ + C$_2$H$_4$) mol Ga^{-1} h^{-1} for γ-Ga$_2$O$_3$/SiO$_2$–H$_2$ after 40 min TOS (Fig. 1C). In contrast, the rates of cracking and
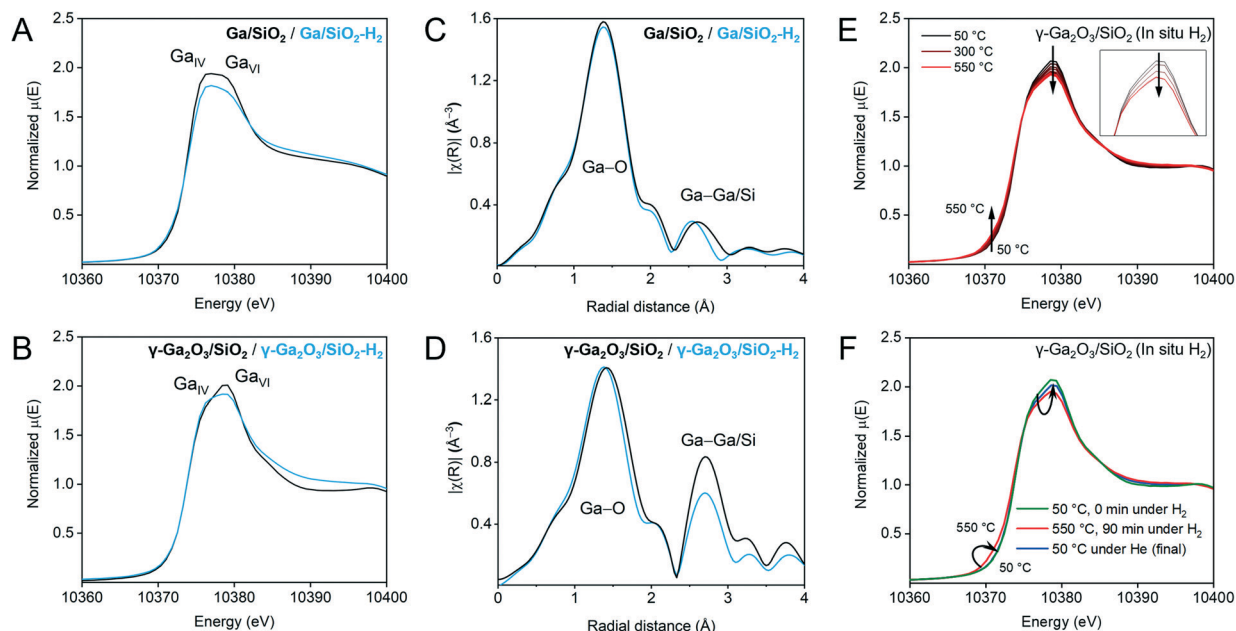
Fig. 2 *Ex situ* Ga K-edge XANES spectra of Ga/SiO$_2$ (A) and γ-Ga$_2$O$_3$/SiO$_2$ (B) before and after H$_2$-treatment (black and blue traces, respectively). EXAFS FT plots (non-phase corrected) before and after H$_2$ treatment (black and blue traces, respectively) for Ga/SiO$_2$ (C) and γ-Ga$_2$O$_3$/SiO$_2$ (D). We note that the *ex situ* XANES and EXAFS data for calcined γ-Ga$_2$O$_3$/SiO$_2$ and Ga/SiO$_2$ have been reported by us previously,[25] and are reproduced here for comparison. (E) Selected normalized traces of *in situ* Ga K-edge XANES during H$_2$ treatment of γ-Ga$_2$O$_3$/SiO$_2$ (50–550 °C). The inset shows changes of the white line and a derivative plot is presented in (Fig. S6†). (F) Comparison of the XANES spectra of γ-Ga$_2$O$_3$/SiO$_2$ before flowing H$_2$ at 50 °C, after 90 min under H$_2$ at 550 °C, and after cooling down under He.

Table 1 Results of EXAFS fittings. Fittings of calcined γ-Ga$_2$O$_3$/SiO$_2$ and Ga/SiO$_2$ have been reported previously and are provided here for comparison in square brackets.[25] Uncertainties determined by least-squares minimization are given in parenthesis. Fixed values are marked by an asterisk. See Table S2† for fittings that include Ga–Si paths

Material	Path	CN	Distance (Å)	σ^2 (Å^2)	R-Factor
γ-Ga$_2$O$_3$/SiO$_2$–H$_2$	Ga–O	5.4(1) [5.4(5)]	1.87(1) [1.89(1)]	0.011* [0.011*]	0.004
	Ga–Ga$_1$	1.7(2) [2.0(1)]	2.98(1) [2.99(1)]	0.009* [0.009]	
	Ga–Ga$_2$	2.3(3) [3.0(1)]	3.37(1) [3.38(1)]	0.009* [0.009]	
Ga/SiO$_2$–H$_2$	Ga–O	5.7(3) [5.7(9)]	1.85(1) [1.86(1)]	0.011* [0.011*]	0.016
	Ga–Ga$_1$	1.0(1) [2.0(1)]	2.91(2) [2.97(1)]	0.011* [0.011]	

propene formation, and the selectivity to propene are similarly low for Ga/SiO$_2$–H$_2$ and Ga/SiO$_2$, although these catalysts show no deactivation with time on stream (Fig. 1A and B).

In situ thermogravimetric analyses (TGA) were carried out under PDH reaction conditions for the H$_2$-treated catalysts and compared to those of the calcined catalysts obtained in our previous work.[25] The amount of coke deposited (g coke g Ga^{-1}) after 104 minutes TOS is *ca.* 25% lower for γ-Ga$_2$O$_3$/SiO$_2$–H$_2$ relative to γ-Ga$_2$O$_3$/SiO$_2$ (0.09 *vs.* 0.12 g coke g^{-1} Ga). Ga/SiO$_2$ and Ga/SiO$_2$–H$_2$ did not deposit any detectable amounts of coke.

Ga K-edge XAS

The local environment and the oxidation state of Ga in γ-Ga$_2$O$_3$/SiO$_2$–H$_2$ and Ga/SiO$_2$–H$_2$ were evaluated using Ga K-edge XANES and compared to the reported results of

calcined γ-Ga$_2$O$_3$/SiO$_2$ and Ga/SiO$_2$.[25] The H$_2$-treated catalysts were measured *ex situ* in air tight conditions. The white-line features at *ca.* 10 375 and 10 379 eV have been attributed to tetrahedral and octahedral, Ga$_{IV}$ and Ga$_{VI}$ sites, respectively.[25,27,39] Yet the interpretation of the XANES spectra, especially for the H$_2$-treated Ga$_2$O$_3$/SiO$_2$ materials, is not straightforward since the position of the white line peaks is affected by the coordination number and symmetry of the Ga sites, as well as the oxidation state of Ga and the ligand type (–O– or –H).[23,40,41] A broad white-line in Ga/SiO$_2$ was previously related to the non-crystalline nature of this material, *i.e.*, only a short range order with different type of sites (different coordination environment) is present in this material.[25] In the spectrum of Ga/SiO$_2$, the feature attributed to the Ga$_{IV}$ site has a slightly higher intensity than that of the Ga$_{VI}$ site (Fig. 2A). The intensity of the white-line peaks in Ga/SiO$_2$–H$_2$ is lower compared to Ga/SiO$_2$, while the Ga$_{IV}$ feature is slightly more intense than the Ga$_{VI}$ feature,

suggesting a change in Ga coordination after H_2 treatment (Fig. 2A). Likewise, the Ga_{IV} feature increases and the Ga_{VI} feature decreases in γ-Ga_2O_3/SiO_2–H_2 relative to γ-Ga_2O_3/SiO_2 (Fig. 2B). The edge position (determined from the maximum in the derivative plot) is 10 374 eV for all studied materials. Thus, *ex situ* Ga K-edge XANES data does not indicate a reduction of Ga^{3+} sites in the H_2 treated materials, yet it suggests a change in their local structure.

We further analyze the local structure around Ga in Ga/SiO_2–H_2 and γ-Ga_2O_3/SiO_2–H_2 and compare it to that of the calcined catalysts using extended X-ray absorption fine structure (EXAFS). Similar to the calcined catalysts, the H_2-treated catalysts display two main peaks in the range of 1–3 Å (non-phase corrected EXAFS plots are presented in Fig. 2C and D) whereby the first peak corresponds to Ga–O and the second peak to Ga–Ga coordination spheres. Modelling of the EXAFS Fourier transformed (FT) data for Ga/SiO_2–H_2 was carried out using a simplified model including one (average) Ga–O path and one Ga–Ga path, while fitting of the EXAFS FT data of γ-Ga_2O_3/SiO_2–H_2 relied on one Ga–O path and two Ga–Ga paths (Fig. S1,† Table 1). Note that the second coordination sphere may also contain contributions from a Ga–Si path, and including a Ga–Si path to the fitting of the EXAFS spectra of Ga/SiO_2–H_2 decreases the *R*-factor (*i.e.* the fractional misfit) notably relative to the fitting that considers only Ga–Ga paths (*i.e.*, from 0.016 to 0.003, Fig. S10, Table S2†). This result is consistent with the presence of gallosilicate species in Ga/SiO_2–H_2 that yield strong BAS (*vide infra*). In contrast, no abundant BAS are detected in γ-Ga_2O_3/SiO_2–H_2 and, in line with this result, the inclusion of a Ga–Si path to fit the EXAFS spectrum of γ-Ga_2O_3/SiO_2–H_2 improves the *R*-factor only slightly, *i.e.* it decreases from 0.004 to 0.002. The σ^2 values (*i.e.*, the mean square relative displacement of the nearest-neighbor atoms around Ga) were fixed to allow a comparison of the materials, *i.e.*, to avoid the high correlation between σ^2 and coordination number (CN). Notice that an increase in the NPs disorder (due to defects or amorphization) can lead to both a decrease in CN and an increase in σ^2 of the second coordination sphere. An alternative fitting using a fixed CN and a variable σ^2 is discussed in the ESI† (Tables S3 and S4).

According to the fittings, the average Ga–O distance in γ-Ga_2O_3/SiO_2–H_2 is 1.87 Å, which is lower by 0.02 Å than in γ-Ga_2O_3/SiO_2 (Table 1).[25] This decrease can be related to a higher relative fraction of Ga_{IV} sites in γ-Ga_2O_3/SiO_2–H_2 as indicated by the XANES data.[39] However, there is no detectable decrease in the coordination number of the first shell, possibly due to the large uncertainties in determining small variation in CN. However, a more notable change in CN occurs in the second coordination sphere, *i.e.*, the CNs of the Ga–Ga shell in γ-Ga_2O_3/SiO_2–H_2 are lower than in γ-Ga_2O_3/SiO_2 (Fig. 2D and S1,† Table 1). This result can be explained by an increased disordering (such as the creation of defects and/or partial amorphization) of the gallia phase in γ-Ga_2O_3/SiO_2–H_2. Indeed, Ga/SiO_2 with mostly amorphous gallia shows even lower intensity of the Ga–Ga coordination

sphere and lower CN values (Table 1). A decrease in the CN of Ga/SiO_2 upon H_2 treatment (Ga/SiO_2–H_2) may be due to a further dispersion of the gallia phase during the H_2 pretreatment of Ga/SiO_2 (*vide infra*).

Changes in the coordination environment of Ga during H_2 treatment of γ-Ga_2O_3/SiO_2 were followed by *in situ* Ga K-edge XAS. γ-Ga_2O_3/SiO_2 was heated in a quartz capillary reactor from 50 to 550 °C under an H_2 flow (10 mL min^{-1}, WHSV = 4.9 h^{-1}) and held at 550 °C for 90 min (Fig. 2E and the derivative plot in Fig. S6†). A subtle feature at *ca.* 10 372 eV develops with increasing temperature, accompanied by a gradual decrease of the white-line intensity (Fig. 2E, inset). Fig. 2F presents XANES spectra of the initial γ-Ga_2O_3/SiO_2 at 50 °C, after 90 min under H_2 at 550 °C, and after the subsequent cooling down to room temperature under He flow (green, red and blue traces, respectively). The room temperature spectrum shows that the low-energy feature disappears after cooling down in He, with an increase in the white line intensity relative to that at 550 °C under H_2; yet the final (after cooling down) white line intensity is slightly lower as compared to the calcined γ-Ga_2O_3/SiO_2. Therefore, *in situ* and *ex situ* XANES are consistent in that the emergence of a low-energy edge feature (at *ca.* 10 372 eV) is observed under H_2 flow at 550 °C but disappears under inert conditions at room temperature.

PDF analysis

To complement the XAS analysis, we further evaluate the structural changes of γ/β-Ga_2O_3 NPs in γ-Ga_2O_3/SiO_2–H_2 by the PDF analysis of X-ray total scattering data. The data collection was carried out *in situ* at 50 °C before and after the treatment of γ-Ga_2O_3/SiO_2 with H_2 at 550 °C. Towards this end, difference PDF (dPDF) analysis was performed by subtracting the background signal of the SiO_2 support from that of γ-Ga_2O_3/SiO_2 and γ-Ga_2O_3/SiO_2–H_2. The reciprocal space data after the subtraction of the SiO_2 signal is shown in Fig. S8.† The signal to noise ratio allowed for a Q_{max} = 16 Å^{-1}. The data reveals subtle differences in the intensity of the γ/β-Ga_2O_3 peaks in γ-Ga_2O_3/SiO_2 and γ-Ga_2O_3/SiO_2–H_2. Turning to real space data, a comparison of the dPDF profiles evidences subtle changes in the local environment of Ga, as reflected by a broadening of the dPDF peaks of γ-Ga_2O_3/SiO_2–H_2 relative to γ-Ga_2O_3/SiO_2, particularly within the range of *ca.* 1.5–6 Å (inset in Fig. S9†). This observation agrees with EXAFS results that suggested that H_2 treatment leads to an increasingly disordered structure of γ-Ga_2O_3/SiO_2–H_2.

Quasi *in situ* XPS

To deepen our understanding of the reducibility of silica-supported, nanocrystalline and amorphous gallia, XPS spectra were acquired after: i) calcination, ii) pretreatment at 550 °C under a flow of H_2 followed by the exposure of the activated material to air before the measurement, and iii) quasi *in situ* treatment under static H_2 (300 mbar, 1 h) at 300 °C and 450 °C (performed at the HPC introduced in the XP

3962 | *Catal. Sci. Technol.*, 2022, **12**, 3957–3968

This journal is © The Royal Society of Chemistry 2022

spectrometer). Calcined γ-Ga_2O_3/SiO_2 features a single peak at 1119.1 eV in the Ga $2p_{3/2}$ region due to Ga^{3+} sites. The low-energy shoulder at *ca.* 1117.2 eV appears in γ-Ga_2O_3/SiO_2–H_2 (*ca.* 12% of the total Ga intensity) even after exposure of the activated material to ambient air during the material transfer (Fig. 3A). Peaks at such low binding energies have been ascribed previously to the formation of either gallium hydrides, Ga^{2+} or Ga^+ species.[20] *In situ* H_2 treatment at 300 °C increases the intensity of this peak to 22% of the total Ga intensity. After H_2 treatment of γ-Ga_2O_3/SiO_2 at 450 °C, an additional peak appears at 1115.7 eV, indicating the formation of Ga^0.[17,42] At this stage, the fitted relative fractions of Ga^0, Ga^+ and Ga^{3+} are *ca.* 21, 37 and 42%, respectively. Calcined Ga/SiO_2 also features a single peak due to Ga^{3+} at 1119.1 eV (Fig. 3B). Ga/SiO_2–H_2 exposed to air during the material transfer shows signatures of reduced Ga sites whereby the fraction of Ga^+ is *ca.* 10%. Performing an *in situ* reduction of Ga/SiO_2 at 300 °C under static H_2 yields Ga^+ and Ga^{3+} species with a distribution of 15 and 85%, whereas the *in situ* reduction of Ga/SiO_2 at 450 °C yields Ga^0, Ga^+ and

Ga^{3+} states with a distribution of 7, 23 and 70% (according to the fits). This comparison reveals that the reduction of Ga^{3+} surface sites proceeds to a larger extend on γ-Ga_2O_3/SiO_2–H_2 compared to Ga/SiO_2–H_2.

Surface acidity studies by ^{15}N DNP SENS and FTIR

γ-Ga_2O_3/SiO_2–H_2 and Ga/SiO_2–H_2 catalysts were exposed to pyridine vapor at room temperature for 20 min, followed by outgassing at 150 °C for 15 min. The respective ^{15}N DNP SENS spectra are presented in Fig. 4A. In these spectra, strong BAS are identified by a peak at *ca.* 205 ppm due to protonated pyridine; furthermore, strong LAS appear at *ca.* 235 ppm, mild LAS at *ca.* 260 ppm, while weak LAS and weak BAS are evidenced with a peak at *ca.* 280 ppm.[43,44] γ-Ga_2O_3/ SiO_2–H_2 reveals two main peaks at *ca.* 237 ppm and 286 ppm. The peak due to strong LAS at 237 ppm was not detected by us previously in γ-Ga_2O_3/SiO_2 after evacuation at 100 °C.[25] The peak at 286 ppm, most likely contains contributions from Py adsorbed on weak LAS of the gallia phase and Py interacting with mild/weak BAS of the silica support.[25] Interestingly, Ga/SiO_2–H_2 shows a similar ^{15}N DNP SENS spectrum compared to that of Ga/SiO_2 (outgassed at 100 °C),[25] and features a major peak due to Py on strong LAS at 236 ppm and a less intense peak due to Py on mild LAS at 260 ppm. In addition, a minor peak due to strong BAS at 206 ppm is present in Ga/SiO_2–H_2 (Fig. 4A). The difference between the intensities of peaks at 283 ppm and 286 ppm in, respectively, Ga/SiO_2–H_2 and γ-Ga_2O_3/SiO_2–H_2 is noteworthy and suggests a sizeable contribution of Py adsorbed on weak Ga-based LAS in γ-Ga_2O_3/SiO_2–H_2 compared to Ga/SiO_2–H_2.[27]
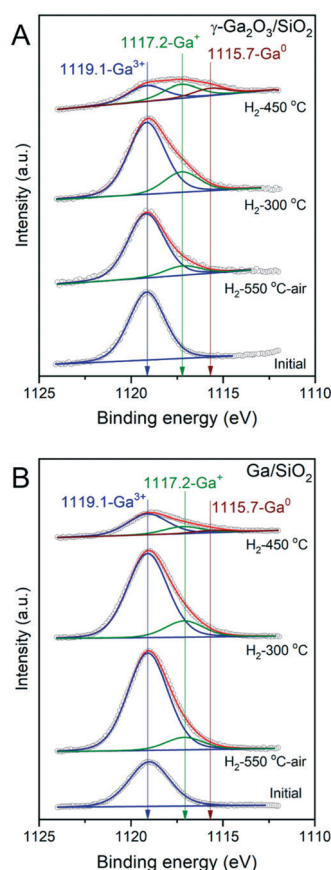

Fig. 3 Deconvoluted Ga 2p XPS spectra of γ-Ga_2O_3/SiO_2 (A) and Ga/ SiO_2 (B). XPS spectra were acquired on calcined materials (initial), after treating them in a reactor under a H_2 flow at 550 °C (H_2-550 °C) followed by their exposure to air during material transfer, and reduced *in situ* at 300 °C or 450 °C in the pretreatment chamber of the XPS instrument (labelled H_2-300 °C and H_2-450 °C, respectively). Fitted blue, green and red traces correspond to XPS features due to Ga^{3+}, Ga^+ and Ga^0 species, respectively.
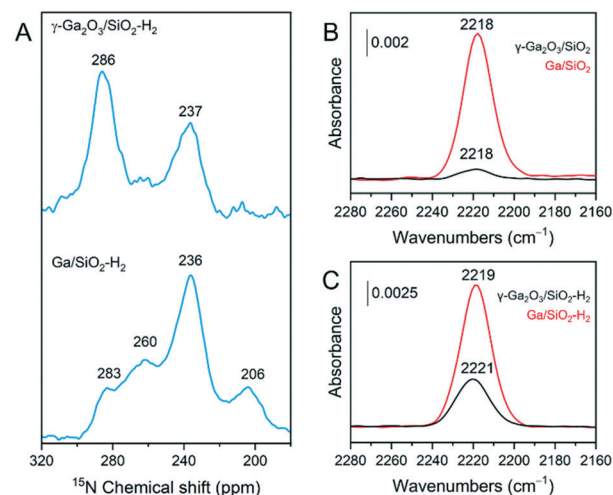

Fig. 4 (A) ^{15}N DNP SENS spectra of ^{15}N-Py adsorbed on γ-Ga_2O_3/ SiO_2–H_2 and Ga/SiO_2–H_2. ^{15}N-Py vapor was adsorbed at room temperature and desorbed under *ca.* 10^{-5} mbar during 15 min at 150 °C. CO adsorption transmission FTIR results for calcined (B) and H_2-treated materials (C). Catalysts were heated to 540 °C and outgassed overnight at *ca.* 10^{-5} mbar. After cooling down to 50 °C, CO was introduced up to a pressure of *ca.* 27 mbar.

This journal is © The Royal Society of Chemistry 2022

Catal. Sci. Technol., 2022, **12**, 3957–3968 | **3963**

Complementary FTIR experiments were carried out to characterize the surface acidity of the studied catalysts. Py adsorption FTIR (Py-FTIR) results show the emergence of a band at *ca.* 1620 cm^{-1} in γ-Ga$_2$O$_3$/SiO$_2$–H$_2$. As this band is absent in γ-Ga$_2$O$_3$/SiO$_2$,[25] the appearance of this band in γ-Ga$_2$O$_3$/SiO$_2$–H$_2$ is consistent with the formation of strong LAS after H$_2$ pretreatment (Fig. S2†). The band at 1620 cm^{-1} is present in Ga/SiO$_2$,[25] and also in Ga/SiO$_2$–H$_2$ (Fig. S2†). On the other hand, bands due to Py on weak/mild BAS located at *ca.* 1595 and 1589 cm^{-1} are removed almost entirely in γ-Ga$_2$O$_3$/SiO$_2$–H$_2$ after outgassing at 100 °C, while these bands are detected in γ-Ga$_2$O$_3$/SiO$_2$ after evacuation at 200 °C.

Adsorption of CO on the four studied catalysts allows to compare the relative intensities of bands due to CO interacting with strong LAS (Fig. 4B and C). CO adsorbed on γ-Ga$_2$O$_3$/SiO$_2$ and Ga/SiO$_2$ gives bands at *ca.* 2218 cm^{-1} for both materials, although the intensity of adsorbed CO is notably stronger on Ga/SiO$_2$ relative to γ-Ga$_2$O$_3$/SiO$_2$. CO adsorbed on Ga/SiO$_2$–H$_2$ gives a spectrum very similar to that of CO adsorbed on Ga/SiO$_2$. In contrast, CO adsorbed on γ-Ga$_2$O$_3$/SiO$_2$–H$_2$ gives a peak shifted slightly to higher wavenumbers, *i.e.* centered at 2221 cm^{-1}, and with a notably higher intensity than in γ-Ga$_2$O$_3$/SiO$_2$, although the intensity is still lower than in Ga/SiO$_2$ or Ga/SiO$_2$–H$_2$.

Hydrogen adsorption FTIR

The heterolytic splitting of H$_2$ on Ga–O linkages was used to identify and characterize surface sites capable to dissociate H$_2$ in the calcined and H$_2$-treated materials. Dissociation of H$_2$ forms GaH and OH sites and the position of the GaH

bands scales with the bond strength and is indicative of the coordination geometry of Ga atoms, *i.e.*, it has been reported that Ga$_{IV}$–H bands are found at *ca.* 2003 cm^{-1} and Ga$_{VI}$–H bands at *ca.* 1980 cm^{-1} (for unsupported gallia).[45] Calcined and *in situ* H$_2$-treated materials were evacuated at 540 °C for 2 h under *ca.* 10^{-4} mbar. Subsequently, adsorption of H$_2$ of *ca.* 70 mbar was conducted at 300, 450 and 540 °C. Fig. 5A and B compare FTIR spectra after dissociation of H$_2$ focusing on the location of the Ga hydride bands of calcined γ-Ga$_2$O$_3$/SiO$_2$ and Ga/SiO$_2$, respectively. Fig. 5C and D show the spectra obtained after dissociation of H$_2$ on γ-Ga$_2$O$_3$/SiO$_2$–H$_2$ and Ga/SiO$_2$–H$_2$, respectively. The dissociation of H$_2$ on γ-Ga$_2$O$_3$/SiO$_2$ gives bands due to gallium hydrides at *ca.* 2037, 2012 and 1986 cm^{-1} (Fig. 5A). In Ga/SiO$_2$, narrower bands are found at higher frequencies at *ca.* 2073, 2058 and 2037 cm^{-1} (Fig. 5B). The dissociation of H$_2$ at 300 °C on γ-Ga$_2$O$_3$/SiO$_2$–H$_2$ produces bands at *ca.* 2073, 2058 and 2041 cm^{-1} (Fig. 5C). These bands resemble closely the gallium hydride bands in Ga/SiO$_2$ (Fig. 5B). Dissociation of hydrogen on γ-Ga$_2$O$_3$/SiO$_2$–H$_2$ at 450 and 540 °C yields an additional broad, lower frequency band at *ca.* 2021 cm^{-1} (Fig. 5C). Except for a slight change of the relative intensities between the different bands, no notable shifts or appearance of new bands were detected on Ga/SiO$_2$–H$_2$ at 300, 450 and 540 °C. When comparing Ga/SiO$_2$–H$_2$ with Ga/SiO$_2$ at the three different temperatures, no substantial band shifts were detected between Ga/SiO$_2$–H$_2$ and Ga/SiO$_2$, although a shoulder at 2021 cm^{-1} becomes notably more intense in Ga/SiO$_2$–H$_2$ (at 450 and 540 °C) and the partial intensities of other bands change after H$_2$ treatment (Fig. 5D).

Lastly, STEM-EDX mappings were used to characterize the dispersion of Ga in the H$_2$-treated catalysts and compare it to calcined catalysts. The images tentatively suggest a higher degree of dispersion of Ga in both H$_2$-treated catalysts relative to the respective calcined catalysts (Fig. S3†).

Discussion

In this work, we aimed to investigate the effect of H$_2$ pretreatment (550 °C, 2 h, undiluted H$_2$) on the catalytic performance and structure of two silica-supported PDH catalysts, one is Ga/SiO$_2$ derived from gallium nitrate containing mostly an amorphous gallia phase, while the other one is a γ-Ga$_2$O$_3$/SiO$_2$ catalyst, obtained by the incipient wetness impregnation of colloidal γ-Ga$_2$O$_3$ nanocrystals onto the SiO$_2$ support. After calcination, γ-Ga$_2$O$_3$ nanocrystals transform partially into β-Ga$_2$O$_3$, yielding SiO$_2$-supported, mixed-phase γ/β-Ga$_2$O$_3$ NPs. Calcined γ-Ga$_2$O$_3$/SiO$_2$ and Ga/SiO$_2$ have been characterized in detail in our previous report.[25]

The Ga/SiO$_2$–H$_2$ catalyst yields a low rate of propene formation (stable at around 3.5 mol C$_3$H$_6$ mol Ga^{-1} h^{-1}), and its selectivity to propene is only *ca.* 50%. This catalyst does not deactivate with TOS and does not deposit any measurable amount of coke. Overall, the activity, selectivity and stability of Ga/SiO$_2$–H$_2$ and Ga/SiO$_2$ are very similar (Fig. 1). In contrast, while the initial activity and selectivity of γ-Ga$_2$O$_3$/
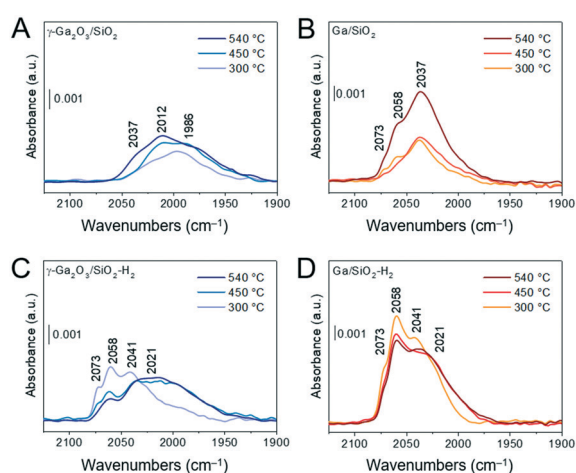

Fig. 5 (A)–(D) Transmission FTIR results of H$_2$ dissociation experiments. Panels show Ga-hydride bands for γ-Ga$_2$O$_3$/SiO$_2$ (A); Ga/SiO$_2$ (B); γ-Ga$_2$O$_3$/SiO$_2$–H$_2$ (C); Ga/SiO$_2$–H$_2$ (D). Materials in self-supported pellets were outgassed for 2 h under *ca.* 10^{-4} mbar at 540 °C. Hydrogen adsorption was conducted at 300 °C, 450 °C and 540 °C at the equilibrium pressure of *ca.* 70 mbar of H$_2$. The hydrogen exposure time at the given temperature was *ca.* 1–2 min, after which the specimen was cooled down to ambient temperature. H$_2$-Treated materials were prepared *in situ* by heating γ-Ga$_2$O$_3$/SiO$_2$ and Ga/SiO$_2$ in *ca.* 130 mbar of H$_2$ at 550 °C for 2 h.

SiO_2–H_2 and γ-Ga_2O_3/SiO_2 are similar (10.3 mol C_3H_6 mol Ga^{-1} h^{-1} and 72%, respectively), after 104 min TOS the activity and selectivity of γ-Ga_2O_3/SiO_2–H_2 are notably higher than that of γ-Ga_2O_3/SiO_2. In addition, γ-Ga_2O_3/SiO_2–H_2 deposits *ca.* 25% less coke as compared to γ-Ga_2O_3/SiO_2. Therefore, H_2 pretreatment attenuates the deactivation of calcined γ-Ga_2O_3/SiO_2 with TOS, primarily owing to a less pronounced decrease of the propene formation rate and the selectivity to propene with TOS, in combination with a lower degree of coking. In what follows, we rationalize the differences in the structure (bulk and surface) between H_2-treated and calcined γ-Ga_2O_3/SiO_2 and Ga/SiO_2 catalysts and relate this structural insight to the improved catalytic performance of γ-Ga_2O_3/SiO_2–H_2 discussed above.

Ex situ XAS (XANES and EXAFS analyses) experiments performed at the Ga K-edge in air-tight conditions suggest a change in the local coordination of Ga that is explained by a higher fraction of Ga_{IV} sites in γ-Ga_2O_3/SiO_2–H_2 than in γ-Ga_2O_3/SiO_2 as seen by a higher intensity of the white line feature at 10375 eV and a decrease in the average Ga–O distance in γ-Ga_2O_3/SiO_2–H_2. Hydrogen treatment of γ-Ga_2O_3/SiO_2 leads to a strong decrease in the coordination number of the Ga–Ga sphere; to a lower extent, this is also observed for Ga/SiO_2. This result indicates that H_2 treatment increases disorder of the supported γ/β-Ga_2O_3 phase in the γ-Ga_2O_3/SiO_2–H_2 catalyst. However, a loss in coherence length in γ-Ga_2O_3/SiO_2–H_2 is not revealed by dPDF analysis, yet this analysis also suggests an increased disorder, particularly in the short range structure (1.5–6 Å). Interestingly, a comparison of the dPDF data for the unsupported γ/β-Ga_2O_3 NPs before and after H_2 treatment (500 °C) shows no detectable differences neither in the short range structure, nor in the medium-to-long range order.[46] STEM-EDX imaging suggests that the agglomeration of the gallia phase on the silica support in both reduced catalysts may be lower relative to the calcined catalysts (Fig. S3†).

In the *in situ* XANES experiments an additional (lower energy) edge feature is observed in γ-Ga_2O_3/SiO_2 under H_2 flow above *ca.* 400 °C. The appearance of such a feature in the XANES spectra (*ca.* 10370–10373 eV) of reduced silica-supported gallia catalysts and Ga-containing zeolites during *in situ* H_2 treatment has been ascribed previously either to the reduction of Ga^{3+} to Ga^+, or Ga^0 species, or to a non-reductive change of the coordination environment of Ga^{3+} sites, including the formation of Ga-hydrides or Ga-alkyls.[16,20,21,23,24] Thus, the observed feature in the *in situ* XANES data of γ-Ga_2O_3/SiO_2 is consistent with a partial reduction of γ/β-Ga_2O_3 in the γ-Ga_2O_3/SiO_2 material and/or a change in the coordination environment of Ga. Interestingly, this feature disappears after the cooling down of γ-Ga_2O_3/SiO_2 under a He flow, in accordance with the lack of this specific low-energy edge feature in the *ex situ* XANES experiments, and may be due to i) the reoxidation of reduced Ga species by the protons of water or surface silanol groups or ii) surface relaxation leading to a loss of low-coordinated Ga_{III} sites formed at high temperature during H_2 treatment.

Analysis of the Ga 2p XPS region confirms clearly the reduction of Ga^{3+} sites in both catalysts after exposing them in the pretreatment chamber to 300 mbar of H_2 for 1 h at 300 and 450 °C. The reduction is evidenced by the appearance of two features at lower BE ascribed to Ga^+ or Ga^0 states. The reduction of Ga^{3+} sites proceeds, according to XPS data fits, to a larger extent in γ-Ga_2O_3/SiO_2–H_2 than in Ga/SiO_2–H_2. The reduction of Ga^{3+} sites is not detected in the Ga 3d region (Fig. S4 and S5†). This is explained by the lower penetration depth for the Ga 2p relative to the Ga 3d XPS region analysis (the inelastic mean free path, λ, is *ca.* 0.9 and 2.4 nm for the Ga 2p and Ga 3d electron energies, respectively), and therefore the formation of Ga^+ or Ga^0 states is mostly a surface phenomenon. Ga^+ or Ga^0 states have been observed previously by XPS of H_2-treated Ga_2O_3/SiO_2 and the formation of metallic Ga^0 was explained by the disproportionation of Ga^+ into Ga^{3+} and Ga^0; it has been suggested that the high vacuum conditions of the XPS measurement may destabilize Ga^+ species and induce disproportionation.[19]

It is interesting to note that Ga^+ sites formed during H_2 pretreatment at 650 °C of a silica-supported amorphous gallia catalyst have been suggested to be inactive in PDH as the reaction rate declined by *ca.* 30% after the H_2 pretreatment.[20] In addition, deactivation of the highly selective (≥93%) single-site [[≡SiO)$_3$Ga–(XOSi≡)] PDH catalyst after 20 h of TOS at 550 °C has tentatively been linked to the reduction of Ga^{3+} surface sites to Ga^+, as seen by the appearance of a low-energy edge feature in the Ga K edge XANES spectrum.[21] In contrast to these results, H_2 pretreatment attenuates the deactivation of γ-Ga_2O_3/SiO_2 with time on stream despite the formation of reduced Ga species. This may be explained by the low amount of reduced Ga species and/or their subsequent disproportionation into Ga^{3+} and Ga^0.

Comparison of the Ga–O sites that are capable of heterolytically dissociating H_2 in γ-Ga_2O_3/SiO_2 and Ga/SiO_2 reveals that three major GaH bands appear in Ga/SiO_2 at higher wavenumbers (2073, 2058 and 2037 cm^{-1}) than in γ-Ga_2O_3/SiO_2 (2037, 2012 and 1986 cm^{-1}). This is consistent with stronger GaH bonds in Ga/SiO_2 which, assuming these Ga^{3+}–O sites are also active in PDH, may be difficult to regenerate by H_2 coupling, leading to a lower catalytic activity of Ga/SiO_2. Interestingly, higher frequency GaH bands that are similar to those in Ga/SiO_2 and Ga/SiO_2–H_2 can be observed in γ-Ga_2O_3/SiO_2–H_2, most clearly when using 300 °C for H_2 dissociation. At higher dissociation temperatures of 450 °C or 540 °C, the main GaH bands in γ-Ga_2O_3/SiO_2–H_2 are similar to those detected in γ-Ga_2O_3/SiO_2 such as the broad lower frequency bands at *ca.* 2021 cm^{-1}, although the bands at the higher wavenumbers, typical for Ga/SiO_2 and Ga/SiO_2–H_2, remain (Fig. 5). Comparison of the GaH bands obtained using silica-supported catalysts of this work with that of unsupported γ/β-Ga_2O_3 NPs after H_2 pretreatment (500 °C) indicates that the more active catalysts feature lower-frequency GaH bands (corresponding to weak GaH bonds), and that the number of distinct GaH bands increases in
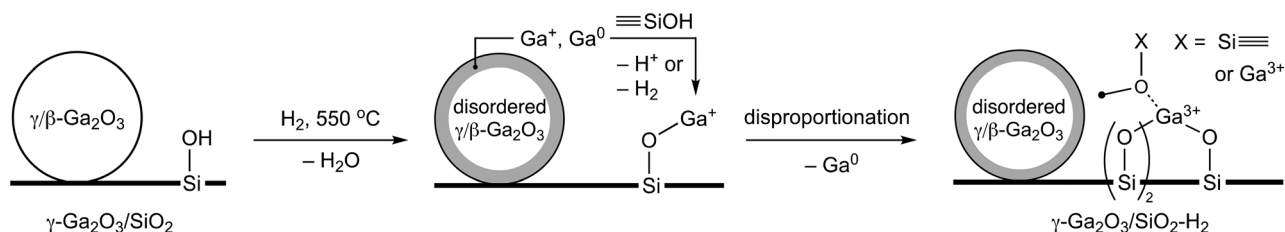
silica-supported catalysts, likely due to the appearance of interfacial sites (with the support).[46] Consequently, the Ga-weight normalized activity of silica-supported catalysts is higher with respect to the unsupported catalysts, *viz.* initial activity of γ-Ga$_2$O$_3$/SiO$_2$ is *ca.* 4.8 times higher relative to γ-Ga$_2$O$_3$, while the surface area of γ-Ga$_2$O$_3$/SiO$_2$ is only *ca.* 2 times higher.

[15]N DNP SENS experiments probe the surface acidity and reveal that the intensity of the peak at *ca.* 286 ppm (desorption temperature 150 °C), which likely has contributions from Py bonded to weak Ga^{3+} LAS and mild/weak BAS (silanols or GaOH sites, which do not protonate pyridine), is notably higher in γ-Ga$_2$O$_3$/SiO$_2$–H$_2$ relative to Ga/SiO$_2$–H$_2$. Py-FTIR experiments show that while Py bonded to mild/weak BAS (bands at *ca.* 1595 and 1589 cm^{-1}) is almost entirely removed from γ-Ga$_2$O$_3$/SiO$_2$–H$_2$ at 100 °C pyridine desorption temperature (T_{des}), the band at 1595 cm^{-1} remains on γ-Ga$_2$O$_3$/SiO$_2$ at T_{des} = 200 °C (Fig. S2†). This may point at the consumption of some of the surface silanols by the reduced Ga species (Ga$^+$ or Ga^0) with the formation of Ga$_{IV}$ sites (*vide infra*). Given that the Ga loadings in γ-Ga$_2$O$_3$/SiO$_2$–H$_2$ and Ga/SiO$_2$–H$_2$ are similar, it is likely that the fraction of weak LAS is higher in γ-Ga$_2$O$_3$/SiO$_2$–H$_2$ than in Ga/SiO$_2$–H$_2$ and this contributes to the higher initial activity of γ-Ga$_2$O$_3$/SiO$_2$–H$_2$ compared to Ga/SiO$_2$–H$_2$. Both γ-Ga$_2$O$_3$/SiO$_2$–H$_2$ and Ga/SiO$_2$–H$_2$ contain a peak due to Py on strong Ga^{3+} LAS at 236–237 ppm. FTIR experiments with CO probe molecule indicate a notably higher intensity of the CO–Ga^{3+} adduct in γ-Ga$_2$O$_3$/SiO$_2$–H$_2$ compared to γ-Ga$_2$O$_3$/SiO$_2$. An increased dispersion of the gallia phase in the H$_2$-treated material may contribute to this increase of intensity of bound CO. However, since a similar increase of dispersion is also observed in Ga/SiO$_2$–H$_2$ but the intensity of adsorbed CO for this material increases only slightly relative to Ga/SiO$_2$, it is likely that the formation of additional strong LAS in γ-Ga$_2$O$_3$/SiO$_2$–H$_2$ is responsible for the increased intensity of bound CO in γ-Ga$_2$O$_3$/SiO$_2$–H$_2$ and the blue shift of the CO band (from 2218 to 2221 cm^{-1}). The formation of strong LAS in γ-Ga$_2$O$_3$/SiO$_2$–H$_2$ is also consistent with Py-FTIR data which shows the emergence of a band at *ca.* 1620 cm^{-1} in γ-Ga$_2$O$_3$/SiO$_2$–H$_2$. This band is weak in γ-Ga$_2$O$_3$/SiO$_2$ but is notably stronger in Ga/SiO$_2$ and Ga/SiO$_2$–H$_2$ (Fig. S2†). We cannot exclude that the formation of these strong LAS is related to the dispersion of Ga after interaction of reduced Ga$^+$ or Ga^0 species with surface silanols (Scheme 1). These reduced

species may disproportionate or get oxidized by H$_2$O forming tetrahedral Ga^{3+} sites. Consistent with this hypothesis is the fact that strong BAS are observed in Ga/SiO$_2$–H$_2$ and previously also in Ga/SiO$_2$, *i.e.*, in materials where an amorphous gallia phase likely co-exists with a small amount of a gallosilicate phase that is responsible for the strong Brønsted acidity. However, we do not observe substantial amounts of strong BAS in γ-Ga$_2$O$_3$/SiO$_2$–H$_2$ (or γ-Ga$_2$O$_3$/SiO$_2$).[25] The higher amounts of reduced Ga species in γ-Ga$_2$O$_3$/SiO$_2$ relative to Ga/SiO$_2$ may be due to the presence of gallosilicate species in Ga/SiO$_2$, which are not reduced in the conditions used in this work.

Overall, the attenuated deactivation of γ-Ga$_2$O$_3$/SiO$_2$–H$_2$ (due to the more stable selectivity to propene and reduced coking with TOS) correlates with an increased disorder of γ/β-Ga$_2$O$_3$ NPs in γ-Ga$_2$O$_3$/SiO$_2$–H$_2$. dPDF analysis of *in situ* X-ray total scattering data suggests that the structural disorder of silica-supported γ/β-Ga$_2$O$_3$ NPs increases during H$_2$ pretreatment and remains only in the local structure of γ/β-Ga$_2$O$_3$. The surface reduction of Ga^{3+} sites is confirmed by the Ga 2p XPS spectra and, potentially, also by *in situ* XANES experiments (appearance of a low-energy edge feature). H$_2$ pretreatment leads to the dissociation of hydrogen and the formation of several gallium hydride sites, some of which are similar in γ-Ga$_2$O$_3$/SiO$_2$–H$_2$, Ga/SiO$_2$–H$_2$ and Ga/SiO$_2$ but are not observed in γ-Ga$_2$O$_3$/SiO$_2$. The additional formation of Ga$_{IV}$ sites in γ-Ga$_2$O$_3$/SiO$_2$–H$_2$ (according to a comparison of the XANES and EXAFS data of γ-Ga$_2$O$_3$/SiO$_2$–H$_2$ and γ-Ga$_2$O$_3$/SiO$_2$) is responsible for more abundant strong Lewis acidity in this material (according to FTIR experiments with CO and Py probe molecules). We propose that those Ga$_{IV}$ sites are mostly due to disordered γ/β-Ga$_2$O$_3$ NPs, yet, there may be a contribution to the formed Ga$_{IV}$-based strong LAS from the interaction of reduced gallium species (Ga$^+$ and/or Ga^0) with silica (Scheme 1), as indicated by the shorter distances of the second coordination sphere of Ga sites after H$_2$ pretreatment. An alternative mechanism for the formation of new Ga$_{IV}$ sites is the disproportionation of Ga$^+$ species (to Ga^{3+} and Ga^0). However, while the interaction of Ga$^+$ and/or Ga^0 is expected to be comparable in both γ-Ga$_2$O$_3$/SiO$_2$–H$_2$ and Ga/SiO$_2$–H$_2$, and the catalytic performance of Ga/SiO$_2$–H$_2$ remains unchanged relative to Ga/SiO$_2$ (in contrast to γ-Ga$_2$O$_3$/SiO$_2$–H$_2$ and γ-Ga$_2$O$_3$/SiO$_2$), the newly formed Ga$_{IV}$ sites in disordered γ/β-Ga$_2$O$_3$ NPs of γ-Ga$_2$O$_3$/SiO$_2$–H$_2$ are likely responsible for the attenuated decrease of the propene selectivity with TOS

Scheme 1 Proposed mechanism for formation of new Ga$_{IV}$ sites in γ-Ga$_2$O$_3$/SiO$_2$–H$_2$ through the reductive disordering of γ/β-Ga$_2$O$_3$ NPs and the subsequent interaction of Ga$^+$ and/or Ga^0 species with the surface silanols.

3966 | *Catal. Sci. Technol.*, 2022, **12**, 3957–3968

This journal is © The Royal Society of Chemistry 2022

for this material. Further, ^{15}N DNP SENS and Py-FTIR data indicate that weak LAS are more abundant in γ-Ga_2O_3/SiO_2–H_2 than in Ga/SiO_2–H_2, and this correlates with the higher initial activity of γ-Ga_2O_3/SiO_2–H_2 and the presence of lower frequency GaH bands in this catalyst. Note that the cracking rate on γ-Ga_2O_3/SiO_2–H_2 has decreased by *ca.* 25% relative to γ-Ga_2O_3/SiO_2, and it remained unchanged (within the experimental error) for Ga/SiO_2–H_2 relative to Ga/SiO_2. Thus, the attenuated loss of activity and propene selectivity with TOS for γ-Ga_2O_3/SiO_2–H_2 (relative to γ-Ga_2O_3/SiO_2) is probably due to the formation of less active but more stable Ga_{IV} sites (due to reduced coking) in the more disordered γ/β-Ga_2O_3 and/or consumption of unselective Ga sites during the H_2 treatment, while the higher initial activity and selectivity of silica-supported catalysts based on γ/β-Ga_2O_3 NPs relative to amorphous gallia is due to the presence of weak LAS in γ/β-Ga_2O_3 NPs.

Conclusions

We reported that H_2 pretreatment (550 °C, 2 h) of γ-Ga_2O_3/SiO_2, a PDH catalyst containing silica-supported nanocrystalline γ/β-Ga_2O_3 NPs, attenuates its deactivation with time on stream. At the same time, H_2 pretreatment does not impact notably the catalytic performance of a Ga/SiO_2 catalyst containing an amorphous gallia phase and a small amount of a gallosilicate phase, identified by its strong Brønsted acidity. We observe that on the silica support, H_2 pretreatment induces a reductive disorder of nanocrystalline γ/β-Ga_2O_3 NPs. This reaction yields additional strong Lewis acid sites, but does not generate strong Brønsted acid sites (that is, it avoids forming a gallosilicate phase). These new sites in the γ-Ga_2O_3/SiO_2–H_2 catalyst may form due to the disproportionation of Ga^+ species (observed by XPS), the anchoring of Ga^+ or Ga^0 species onto silanol groups, and/or an H_2-induced local disordering of nanocrystalline γ/β-Ga_2O_3 NPs; the latter mechanism appears to contribute the most. Our results suggest that the active sites in the silica-supported gallia catalysts based on strong LAS (*i.e.*, Ga_{IV} sites formed after the H_2 pretreatment) are less active but more stable with TOS than weak LAS of γ/β-Ga_2O_3 NPs.

Author contributions

P. C.-F. and A. F. designed the research project and planned the experimental work. P. C.-F. carried out the preparation of materials, characterization and testing of the catalysts, and data analysis. A. I. S. performed hydrogen adsorption FTIR experiments and supervised data interpretation. A. V. Y. carried out ^{15}N DNP SENS experiments, processed the results and contributed to data analysis. I. P. P. and A. V. B. conducted XPS experiments, data processing and analysis. P. M. A. supervised XAS and dPDF experiments and contributed to the data analysis. The data were discussed among all co-authors. P. C.-F. and A. F. wrote the first version of the draft

that was edited by all authors. All authors have given approval to the final version of the manuscript.

Conflicts of interest

The authors declare no conflicts of interest.

Acknowledgements

Notes and references

1 J. J. H. B. Sattler, J. Ruiz-Martinez, E. Santillan-Jimenez and B. M. Weckhuysen, *Chem. Rev.*, 2014, **114**, 10613–10653.

2 Z. P. Hu, D. Yang, Z. Wang and Z. Y. Yuan, *Chin. J. Catal.*, 2019, **40**, 1233–1254.

3 S. Chen, X. Chang, G. Sun, T. Zhang, Y. Xu, Y. Wang, C. Pei and J. Gong, *Chem. Soc. Rev.*, 2021, **50**, 3315–3354.

4 C. Copéret, F. Allouche, K. W. Chan, M. P. Conley, M. F. Delley, A. Fedorov, I. B. Moroz, V. Mougel, M. Pucino, K. Searles, K. Yamamoto and P. A. Zhizhko, *Angew. Chem., Int. Ed.*, 2018, **57**, 6398–6440.

5 S. R. Docherty, L. Rochlitz, P. A. Payard and C. Copéret, *Chem. Soc. Rev.*, 2021, **50**, 5806–5822.

6 A. Bhan and W. N. Delgass, *Catal. Rev.: Sci. Eng.*, 2008, **50**, 19–151.

7 J. R. Mowry, D. C. Martindale and A. H. P. Hall, *Arabian J. Sci. Eng.*, 1985, **10**, 367–375.

8 M. Monai, M. Gambino, S. Wannakao and B. M. Weckhuysen, *Chem. Soc. Rev.*, 2021, **50**, 11503–11529.

9 R. Fricke, H. Kosslick, G. Lischke and M. Richter, *Chem. Rev.*, 2000, **100**, 2303–2405.

10 V. Kanazirev, G. L. Price and G. Tyuliev, *Zeolites*, 1992, **12**, 846–850.

11 M. W. Schreiber, C. P. Plaisance, M. Baumgärtl, K. Reuter, A. Jentys, R. Bermejo-Deval and J. A. Lercher, *J. Am. Chem. Soc.*, 2018, **140**, 4849–4859.

12 N. M. Phadke, E. Mansoor, M. Bondil, M. Head-Gordon and A. T. Bell, *J. Am. Chem. Soc.*, 2019, **141**, 1614–1627.

13 E. Mansoor, M. Head-Gordon and A. T. Bell, *ACS Catal.*, 2018, **8**, 6146–6162.

This journal is © The Royal Society of Chemistry 2022

Catal. Sci. Technol., 2022, **12**, 3957–3968 | **3967**

14 N. M. Phadke, J. Van Der Mynsbrugge, E. Mansoor, A. B. Getsoian, M. Head-Gordon and A. T. Bell, *ACS Catal.*, 2018, **8**, 6106–6126.

15 E. J. M. Hensen, M. García-Sánchez, N. Rane, P. C. M. M. Magusin, P. H. Liu, K. J. Chao and R. A. Van Santen, *Catal. Lett.*, 2005, **101**, 79–85.

16 G. D. Meitzner, E. Iglesia, J. E. Baumgartner and E. S. Huang, *J. Catal.*, 1993, **140**, 209–225.

17 A. I. Serykh and M. D. Amiridis, *Surf. Sci.*, 2009, **603**, 2037–2041.

18 I. Takahara, M. Saito, M. Inaba and K. Murata, *Catal. Lett.*, 2004, **96**, 29–32.

19 A. I. Serykh and M. D. Amiridis, *Surf. Sci.*, 2010, **604**, 1002–1005.

20 V. J. Cybulskis, S. U. Pradhan, J. J. Lovón-Quintana, A. S. Hock, B. Hu, G. Zhang, W. N. Delgass, F. H. Ribeiro and J. T. Miller, *Catal. Lett.*, 2017, **147**, 1252–1262.

21 K. Searles, G. G. Siddiqi, O. V. Safonova and C. Copéret, *Chem. Sci.*, 2017, **8**, 2661–2666.

22 C. Copéret, A. Comas-Vives, M. P. Conley, D. P. Estes, A. Fedorov, V. Mougel, H. Nagae, F. Núñez-Zarur and P. A. Zhizhko, *Chem. Rev.*, 2016, **116**, 323–421.

23 L. Rochlitz, K. Searles, D. F. Nater, S. R. Docherty, D. Gioffrè and C. Copéret, *Helv. Chim. Acta*, 2021, **104**, e2100078.

24 A. Getsoian, U. Das, J. Camacho-Bunquin, G. Zhang, J. R. Gallagher, B. Hu, S. Cheah, J. A. Schaidle, D. A. Ruddy, J. E. Hensley, T. R. Krause, L. A. Curtiss, J. T. Miller and A. S. Hock, *Catal. Sci. Technol.*, 2016, **6**, 6339–6353.

25 P. Castro-Fernández, D. Mance, C. Liu, I. B. Moroz, P. M. Abdala, E. A. Pidko, C. Copéret, A. Fedorov and C. R. Müller, *ACS Catal.*, 2021, **11**, 907–924.

26 W. Jochum, S. Penner, K. Föttinger, R. Kramer, G. Rupprechter and B. Klötzer, *J. Catal.*, 2008, **256**, 268–277.

27 P. Castro-Fernández, M. Kaushik, Z. Wang, D. Mance, E. Kountoupi, E. Willinger, P. M. Abdala, C. Copéret, A. Lesage, A. Fedorov and C. R. Müller, *Chem. Sci.*, 2021, **12**, 15273–15283.

28 M. Chen, J. Xu, F. Z. Su, Y. M. Liu, Y. Cao, H. Y. He and K. N. Fan, *J. Catal.*, 2008, **256**, 293–300.

29 W. Van Beek, O. V. Safonova, G. Wiker and H. Emerich, *Phase Transitions*, 2011, **84**, 726–732.

30 C. S. S. R. Kumar, *X-ray and Neutron Techniques for Nanomaterials Characterization*, Springer Nature, Berlin, 2016.

31 B. Ravel and M. Newville, *J. Synchrotron Radiat.*, 2005, **12**, 537–541.

32 J. Åhman, G. Svensson and J. Albertsson, *Acta Crystallogr., Sect. C: Cryst. Struct. Commun.*, 1996, **52**, 1336–1338.

33 P. J. Chupas, K. W. Chapman and G. J. Halder, *J. Am. Chem. Soc.*, 2011, **133**, 8522–8524.

34 P. Juhás, T. Davis, C. L. Farrow and S. J. L. Billinge, *J. Appl. Crystallogr.*, 2013, **46**, 560–566.

35 A. Zagdoun, G. Casano, O. Ouari, M. Schwarzwälder, A. J. Rossini, F. Aussenac, M. Yulikov, G. Jeschke, C. Copéret, A. Lesage, P. Tordo and L. Emsley, *J. Am. Chem. Soc.*, 2013, **135**, 12790–12797.

36 A. Zagdoun, A. J. Rossini, D. Gajan, A. Bourdolle, O. Ouari, M. Rosay, W. E. Maas, P. Tordo, M. Lelli, L. Emsley, A. Lesage and C. Copéret, *Chem. Commun.*, 2012, **48**, 654–656.

37 J. H. Scofield, *J. Electron Spectrosc. Relat. Phenom.*, 1976, **8**, 129–137.

38 P. Castro-Fernández, M. V. Blanco, R. Verel, E. Willinger, A. Fedorov, P. M. Abdala and C. R. Müller, *J. Phys. Chem. C*, 2020, **124**, 20578–20588.

39 K. Nishi, K. Shimizu, M. Takamatsu, H. Yoshida, A. Satsuma, T. Tanaka, S. Yoshida and T. Hattori, *J. Phys. Chem. B*, 1998, **102**, 10190–10195.

40 K. Groden, F. D. Vila, L. Li, S. R. Bare, S. L. Scott and J.-S. McEwen, *J. Phys. Chem. C*, 2021, **125**, 27901–27908.

41 L. Yang, J. L. Bourque, J. A. McLeod, P. Shen, K. M. Baines and L. Liu, *Inorg. Chem.*, 2017, **56**, 2985–2991.

42 R. Carli and C. L. Bianchi, *Appl. Surf. Sci.*, 1994, **74**, 99–102.

43 I. B. Moroz, K. Larmier, W.-C. Liao and C. Copéret, *J. Phys. Chem. C*, 2018, **122**, 10871–10882.

44 W. R. Gunther, V. K. Michaelis, R. G. Griffin and Y. Roman-Leshkov, *J. Phys. Chem. C*, 2016, **120**, 28533–28544.

45 S. E. Collins, M. A. Baltanás and A. L. Bonivardi, *Langmuir*, 2005, **21**, 962–970.

46 P. Castro-Fernández, D. Mance, C. Liu, P. Abdala, E. Willinger, A. A. Rossinelli, A. I. Serykh, E. A. Pidko, C. Copéret, A. Fedorov and C. R. Müller, *J. Catal.*, 2022, **408**, 155–164.

3968 | *Catal. Sci. Technol.*, 2022, **12**, 3957–3968

This journal is © The Royal Society of Chemistry 2022